*Journal of The Electrochemical Society*, **166** (13) A2849-A2859 (2019) 

# How to Cool Lithium Ion Batteries: Optimising Cell Design using a Thermally Coupled Model

**Yan Zhao,[1] Laura Bravo Diaz,[1] Yatish Patel,[1,2] Teng Zhang,[3,*] and Gregory J. Offer[1,2,*,z]**

[1]*Department of Mechanical Engineering, Imperial College London, London SW7 2AZ, United Kingdom*
[2]*The Faraday Institution, Quad One, Becquerel Avenue, Harwell Campus, Didcot, OX11 0RA, United Kingdom*
[3]*Department of Mechanical Engineering, University of Surrey, Guildford GU2 7XH, United Kingdom*

Cooling electrical tabs of the cell instead of the lithium ion cell surfaces has shown to provide better thermal uniformity within the cell, but its ability to remove heat is limited by the heat transfer bottleneck between tab and electrode stack. A two-dimensional electro-thermal model was validated with custom made cells with different tab sizes and position and used to study how heat transfer for tab cooling could be increased. We show for the first time that the heat transfer bottleneck can be opened up with a single modification, increasing the thickness of the tabs, without affecting the electrode stack. A virtual large-capacity automotive cell (based upon the LG Chem E63 cell) was modelled to demonstrate that optimised tab cooling can be as effective in removing heat as surface cooling, while maintaining the benefit of better thermal, current and state-of-charge homogeneity. These findings will enable cell manufacturers to optimise cell design to allow wider introduction of tab cooling. This would enable the benefits of tab cooling, including higher useable capacity, higher power, and a longer lifetime to be possible in a wider range of applications.
 [DOI: 10.1149/2.0501913jes]

Manuscript submitted June 17, 2019; revised manuscript received August 7, 2019. Published August 21, 2019.

Electrification of transport continues to be an integral part of the mission to reduce greenhouse gas emissions and local air pollution. Electric vehicles (EVs) stock continues to see significant growth with the global EVs stock surpassed 3 million vehicles in 2017, a 56% expansion compared with 2016.[1] One of the key technological challenges is to make the lithium ion (Li-ion) battery pack cheaper and longer-lasting.

To maximise the performance of a battery pack over its lifetime, the cell temperature needs to be carefully managed. Significant deviations from ambient conditions can lead to reduced performance, accelerated degradation and in extreme cases catastrophic failure, i.e. thermal runaway.[2–8] To counter these challenges, the temperature of the EV battery pack is normally managed by using thermal management system (TMS).[9–14] The main purpose of the TMS is to maintain the overall temperature in an optimal window as well as maintain a uniform temperature between cells and within the cells.

Under aggressive usages such as fast charging, thermal gradients can often arise due to heat transfer limitations.[15–18] These limitations depend on the choice of the TMS method as well as cell design. Cells can be thermally managed through different surfaces, namely electrode-stack surface, electrical terminals (tabs) or both.[12,19,20] In our previous work, Hunt et al. showed that the choice of the TMS method can have a significant effect on cell performance and lifetime.[19] It was shown that tab cooling can reduce the usable capacity degradation rate by a factor of three to surface cooling under an aggressive cycling condition. Subsequent modelling work by Zhao et al. showed that surface cooling induced a significant thermal gradient across the cell thickness leading to current and State-of-Charge (SoC) inhomogeneity.[21] As a result, colder electrode layers were at significantly different SoCs than the hotter layers, so the true capacity of the cell could not be fully utilised. It was hypothesised that the significant temperature inhomogeneity would lead to localised degradation in the hotter cell layers due to the positive feedback of higher temperature, lower impedance and larger current. In comparison, tab cooling provided a much smaller thermal gradient across the cell thickness but could not keep the cell average temperature as low. The model identified that the heat transfer 'bottlenecks' are the cross-sectional areas (width × thickness plane) of the tabs and the thermal resistance induced by the welding point between the tab and the electrode stack.[4,21] It was hypothesised that wider tabs can improve heat transfer from the electrode stack to the tabs. Therefore, there is a need to further optimise cell design to allow tab cooling to be utilised more effectively in a wider range of applications.

Numerous studies have analyzed the effect of cell physical and geometrical parameters on the cell performance.[22–27] These parameters include the aspect ratio, tab position and electrode-stack thickness. A majority of these studies focus on the uneven current flow – and consequently temperature and SoC inhomogeneity - within the electrode plane caused by the finite electrical resistance of current collectors.[24,25,28] For example, Samba et al. investigated the effect of tab location on the cell performance and concluded that symmetrical tab position and wider tabs improve the homogeneity. These conclusions agree with the findings of Kim et al. and Rieger et al.[25,26] However, these studies only considered forced air convective thermal boundary conditions that are not representative of the more prevalent liquid-cooling thermal boundary conditions for EV battery packs. As shown in our previous work,[19,21] the inhomogeneity caused by the external thermal boundary conditions (e.g. TMS choice) can be much more dominant under aggressive usage. To fully understand the impact of the cell geometrical parameters on the cell performance, the thermal gradient induced and its consequence, they must be studied in the direction of the dominant heat transfer pathway representative of the external thermal boundary conditions. While there is a significant effort in optimising cells for electrochemical performance, there is a very limited focus on optimising the cell geometrical parameters for thermal performance, i.e. improved heat transfer rate to the TMS.

A model-based approach is often employed due to the difficulties encountered in manufacturing/acquiring cells with the desired geometrical properties.[27,29–31] However, the critical parameters (such as tab position and size) identified by these models are often not validated with measurements using real cells.

In this work, custom made Li-ion cells with different tab positioning and width were used to validate hypotheses on ways to open up the heat transfer bottleneck. Peltier-element-controlled test rigs for tab cooling and surface cooling were built to assess the thermal and electrical performance of different tab designs. Two-dimensional thermal electrical models were parameterised and validated. The models were used to explore internal states such as temperature, current, and SoC distributions across the thickness of the cell. In addition, the model was used to explore the most effective ways to remove the thermal 'bottleneck' for a tab cooled system. The effectiveness of changing geometrical parameters such as tab width, tab thickness and current collector thickness was assessed. Furthermore, a 'virtual' automotive cell was modelled to investigate the effectiveness of using tab cooling for large-format cells.

*Electrochemical Society Member.
[z]E-mail: gregory.offer@imperial.ac.uk

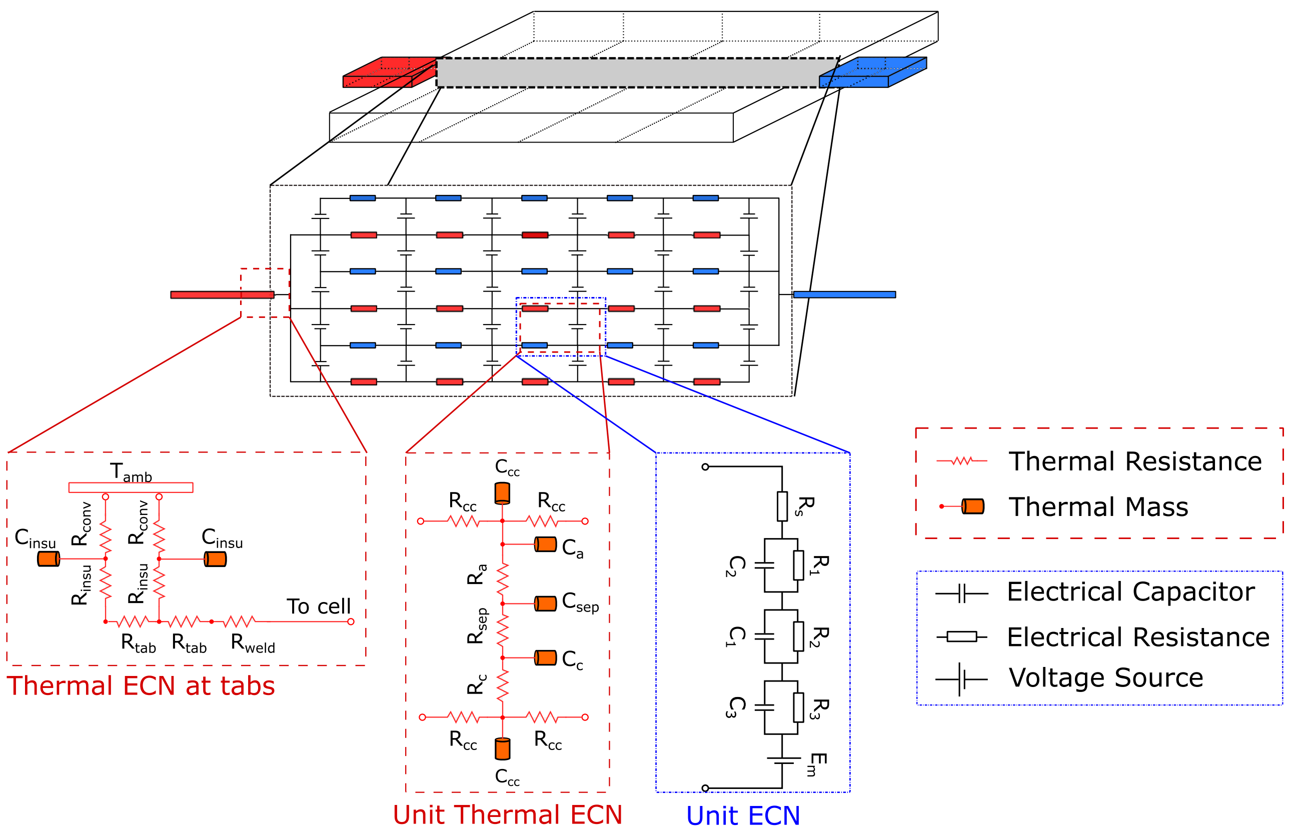


**Figure 1.** Figure schematic for the 16 Ah custom made cells. Adapted from Figure 1 by Zhao et al.[21] under the terms of the Creative Commons Attribution 4.0 License (CC BY).

## Model Development

The modelling framework used in this work is based on the two-dimensional electro-thermal model developed in our previous work.[21] The model was developed in MATLAB R2017a using Simulink (v8.8) and Simscape toolbox (v4.1).

The modelling framework is developed based on the work of Newman, Tiedemann, Gu and Kwon (NTGK) et al.[32–34] Figure 1 shows a schematic of the modelling framework. The detailed model description can be found in Zhao et al.[21] The model simulates the length (L) and thickness (T) plane. The dimension across the width (W) is not included as it is assumed the thermal gradient is minimum.[21]

In the simulation domain (L × T), the cell is discretised into identical unit cells and a 2D network is formed by connecting unit cells. Within each unit cell, an Equivalent Circuit Network (ECN) model is used to simulate voltage and current behavior. A thermal ECN is also used in each unit cell to simulate the heat transfer between cell components (anode, cathode, current collectors and separators). Overall, there are 30 nodes distributed evenly throughout the simulation domain, with 6 discretisation distributed along length direction and 5 discretisation through the cell thickness.

The boundary surfaces (i.e. electrode stack surfaces (W × L) and tabs) are applied with various thermal boundary conditions to simulate various thermal management strategies. These allow used to simulate the heat transfer between the cell and the environment. As with our previous work, particular attention was paid to model the non-cell-stack components (e.g. tab weld) as well as the thermal boundary conditions.

## Experimental

Three variants of pouch-type custom made cells manufactured by Customcells Itzehoe GmbH were used for this work. All variants contain a graphite anode and a $LiNi_{0.6}Mn_{0.2}Co_{0.2}O_2$ (NMC-622) cathode. All variants have identical electrode stack (cathodes, anodes. current collectors and separators). All variants have a rated capacity of 16 Ah. The stacks have overall dimensions of L 117 mm × W 101 mm × T ~11.5 mm.

The tab position and tab size of the three variants are shown in Figure 2. The baseline design, S30, has the cell tabs positioned at the same side with a width 30 mm at each tab as shown in Figure 2a. The first variant, C30, has the cell tabs positioned at the counter side of the cell with the same width as the S30 cell. The last variant, C70, is shown in Figure 2c, the cell tabs are positioned at the counter side of the cell with a width of 70 mm. The detailed dimensions are shown in Table I.

For all ECM parameterisation experiments, the ambient temperature is controlled by forced air convection using a Binder Cooling Incubator (Model: KB23). For all the other experiments, the ambient temperature is controlled by using an ESPEC environmental chamber (Model: BPL-3). In the thermal characterisation experiments, the temperature of different cell surfaces (electrode surfaces and tabs) was controlled by using liquid-cooled heatsinks. The temperature of the coolant is controlled by employing an immersion circulator (Model: PC200 manufactured by Thermo Scientific) with liquid temperature stability of 0.01°C. The temperature on the various cell surfaces was measured using K-type thermocouples. Thermocouples were bonded on the cell electrode-stack surface and tabs to monitor temperature rise

**Table I. The tab size dimension, thickness and position.**

| | S30 | C30 | C70 |
|---|---|---|---|
| Tab width [mm] | 30 | 30 | 70 |
| Tab length [mm] | 21 | 21 | 21 |
| Tab thickness [mm] | 0.2 | 0.2 | 0.2 |
| Position | Same side | Counter side | Counter side |

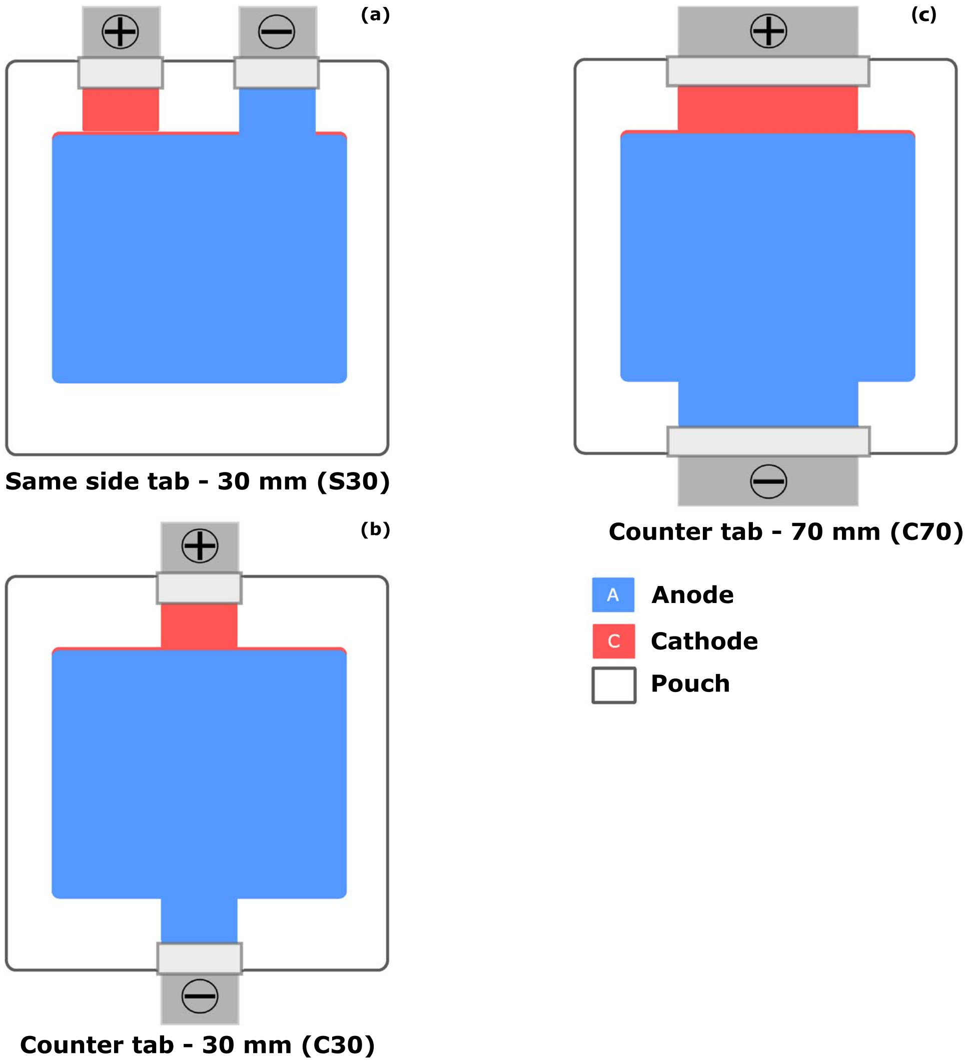


**Figure 2.** Custom made cell variant: (a) Same side tabs −30 mm (S30), (b) Counter side tabs – 30mm and (c) Counter side tabs −70 mm.

during the discharge process. The thermocouple data was recorded using the temperature data acquisition module manufactured by National Instrument (Model: NI 9213 temperature input module and CompactDAQ 9178 chassis).

For the experiments under TMS, the temperature at the tab or electrode stack surface was controlled by the bespoke temperature control rigs. The detailed design of these test rigs can be found in our previous work.[19,35]

The cells were tested by using a Maccor (Model: Series 4000) battery tester. The 'near-adiabatic' condition at surfaces without cooling applied was created by covering exposed cell surfaces with thermal insulation material, Superwool 607 Fibre blanket (manufactured by Morgan Advanced Materials).

***Model parameterisation.—*** *ECN parameterisation.*—The ECN model was parameterised by using the Pulse Discharge (PD) method, the same procedure as described in our previous work.[21] The procedure involves applying discharge pulse at the constant current rate of 16 A and monitoring the cell voltage in the subsequent 2h resting period. This procedure is repeated from SoC 100% to SoC 0% in steps of 1% between 100% - 90% SoC and 10% - 0% SoC, and in steps of 5% between 90% and 10% SoC range. The procedures were conducted in environmental temperatures of 10ºC, 20ºC, 30ºC and 40ºC.

The details of the procedure and the corresponding parameter estimation methodology can be found in our previous work and Jackey et al.[21,36,37] The parameters obtained at the cell level are scaled down for the individual cell section. To allow this calculation, it was assumed the cell anode, cathode, separator and electrolyte filling are uniform across the cell stack at the start of the life. The re-scaling of the full parameter is shown in Equation 1 and Equation 2.

$$\mathrm{R}_{i,e}=\mathrm{R}_{i,cell}\cdot N \quad [1]$$

$$C_{i,e}=\frac{C_{i,cell}}{N} \quad [2]$$

Where $\mathrm{R}_{i,e}$, $C_{i,e}$ are the resistance and capacitance of the individual cell section; $N$ is the total number of sections in the model; and $\mathrm{R}_{\mathrm{i,cell}}$ and $C_{i,cell}$ are resistance and capacitance at the cell level.

*Thermal parameters.*—The thermal conductivity and specific heat capacity for cell-stack components were taken from literature, as shown in Table II.[19,38] The entropic heat generation was included as well as all other irreversible heat sources. The physical parameter of cell components was provided by the supplier. The cell specific heat capacity was measured using an Accelerating Rate Calorimeter (ARC) manufactured by Thermal Hazard Technology (THT), to be 1.125 J/kg·k with a standard deviation of 0.049 J/kg·k. The measured specific heat capacity was used to verify the overall modelled value, which is calculated from the property of the individual components. The model has an overall specific capacity of 1.118 J/kg·k, a 0.62% deviation from the measurement.

**Table II. The cell electrode stack component dimensions.**[19,38]

| | Width [mm] | Length [mm] | Thickness [μm] | No. of Layers | Thermal conductivity[$Wm^{-1}K^{-1}$] | Specific heat capacity[$J\ kg^{-1}K^{-1}$] |
|---|---|---|---|---|---|---|
| Cathode | 98 | 115 | 51 | 74 | 1.04[31] | 1058 |
| Anode | 100 | 117 | 60 | 75 | 1.58[31] | 1437[31] |
| Separator | 101 | 119 | 20 | 76 | 0.34[31] | 1978[31] |
| Copper current collector | 100 | 117 | 10 | 38 | 398[31] | 385[31] |
| Aluminium current collector | 98 | 115 | 20 | 37 | 238[31] | 903[38] |
| Casing | n/a | n/a | 112 | 2 | 238[31] | 903[38] |

The non-stack cell components such as the tab weld point thermal resistances were characterised by conducting the thermal transient experiments. Thermal boundary parameters such as convective heat transfer coefficient, thermal conductivity of thermal paste and thermal insulation were also calibrated by using these tests. Five transient heat experiments were conducted. The details of these can be found in our previous work.[21] No electric current was applied for the thermal transient test. In each test, the cell was allowed to reach the thermal equilibrium in the 30ºC environmental chamber. The heatsink with coolant temperature at 15ºC was placed on the target surface at the start of each test. The surfaces are positive and negative tabs of the C30 cell, positive and negative tabs of the C70 cell and the electrode-stack surface of the S30 cell. One surface was tested in each test, and the transient temperature profile was measured. The model was then used to fit the experimental result to calibrate the parameters shown in Table III.

## Results and Discussion

***Cell performance.***—Figure 3 shows the discharge curve of the three variants under the discharge rate of the C/10 (1.6 A). It was assumed the discharge current was sufficiently low to not induce any cell temperature change such that the resulting discharge voltage to allow comparison of total charge stored and shape of discharge curve between variants. All three cells show similar capacities with a maximum difference of 0.5 Ah (2.8%). The differences between cells can be attributed to manufacturing tolerance.

***Thermal transient tests.***—The thermal transient tests described in Thermal parameters section are used to demonstrate the improvement in the heat transfer rate from using wider tabs. The cell was at 30ºC at the beginning of each test. The coolant temperature flowing through the heatsink was controlled at 15ºC. The heatsink was then placed onto the tab surface at the start of the test. The test was repeated for positive and negative tabs individually for each the cell variants.

Figure 4 shows temperature measurements during the test from the tabs, the cell surface (centre) and the coolant. Figure 4a shows the transient temperature profile for cooling the negative tabs. Compared to the C30 cell, the C70 cell temperature is 2.3ºC lower at the centre of the surface at a steady state. At the negative tab, the C70 cell temperature is 1.5ºC lower in comparison. Figure 4b shows the temperature transient profile for cooling the positive tabs. A comparable temperature difference exists between the C70 and the C30 cell, with the C70 cell temperature being 2ºC lower at the surface and 0.7ºC lower at the positive tab. In summary, the wider tab reduces the equivalent thermal resistance of conducting heat through cell tabs. The results show the cell with wider tabs (C70) has reduced thermal resistance when tab cooling is employed.

Compared to the positive tab tests, the cooling tests for the negative tab result in a lower steady-state temperature, approximately 1ºC at the cell surface. This is expected as the negative tab and the current collector are made of copper, which has a higher thermal conductivity compared to the positive tab material, aluminum.

***Performance under thermal management system.***—The thermal transient test has shown that the cooling performance of TMS based on tab cooling can be potentially improved by wider electrical tabs. In this section, the cells were tested with TMS applied.

For the baseline test, one face of the S30 was cooled. It was assumed that all variants will perform similarly under surface cooling due to the identical heat transfer area. Tab cooling was then applied to all three variants (S30, C30 and C70).

Figure 5 shows a comparison of the average cell temperature under different TMS. In these tests, the cells were allowed to reach OCV of 4.2 V by charging at a constant current rate 1C (16 A) till 4.2 V, followed by a constant voltage period until the current is less than 0.01C (0.16 A) and were then allowed to rest for 2h. The cells were allowed to thermally equilibrate for 3 hours before the current was applied. The cells were then discharged at a constant current rate of 5C (80 A) until 2.7 V, followed by a constant current charging at rate of 2C (32 A) until 4.2 V.

As shown in Figure 5, the surface cooled S30 cell has the lowest peak temperature of 33.3°C, occurring at the end of the discharge. The discharge was terminated earlier than any other cell. This could be caused by the lower average temperature during the discharge, which led to a higher impedance and a lower usable capacity.

**Table III. Calibrated thermal boundary parameters.**

| Calibrated parameters | Thermal conductivity[$Wm^{-1}K^{-1}$] | Thickness [mm] |
|---|---|---|
| Thermal insulation | 0.08 | 8 |
| Thermal contact at positive tab weld | 150 | 4.2 |
| Thermal contact at negative tab weld | 205 | 4.2 |
| Thermal paste | 3.97 | 0.2 |

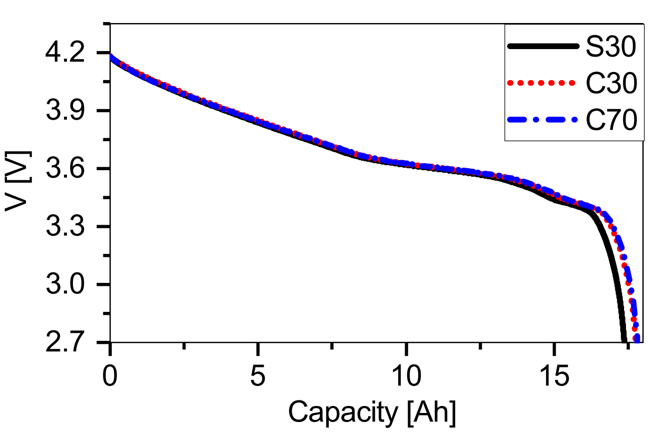


**Figure 3.** Discharge curve of the three variants (S30, C30 and C70) at 0.1 C.

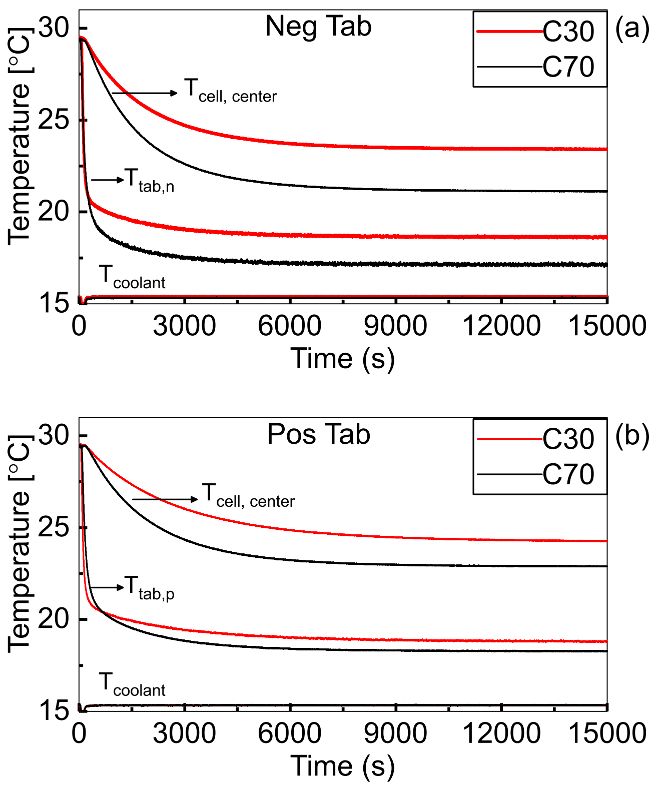


**Figure 4.** Thermal transient test at tabs: (a) Negative tab cooling, (b) Positive tab cooling.

For the tab cooled cells with a narrower tab (S30 and C30), the peak temperature was 45.5°C and 44.5°C respectively at the end of discharge. S30 and C30 cells also show a similar average temperature under this load. The C30 cell has shown a slightly larger useable capacity by 0.6 Ah. The C70 tab cooled showed a significant reduction in the peak temperature by 6°C compared to the cells with 30 mm tabs. This is consistent with the results shown in the thermal transient characterisation in Figure 4. It is clear that wider tabs provide better heat transfer through the tabs. However, it is difficult to quantify this improvement experimentally as the peak temperature is dependent on heat transfer as well as heat generation. Cell-to-cell heat generation difference is difficult to quantify experimentally. Therefore, a model is used to assess the effect of changing tab width.

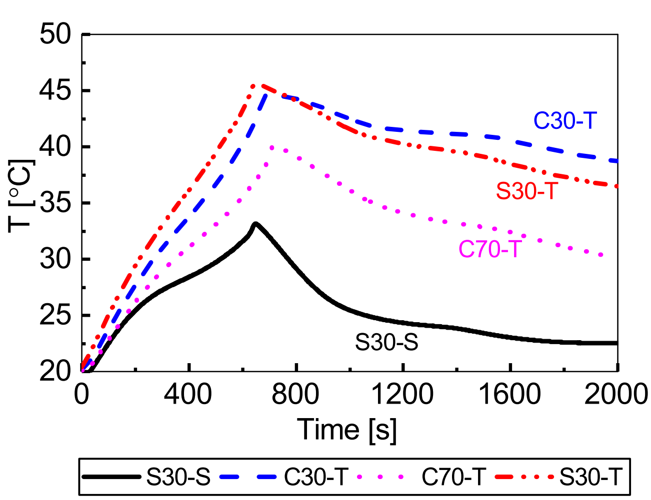


**Figure 5.** Cell temperatures over a 5C discharge followed by a 2C charge under different TMS.

While wider tabs provide a noticeable improvement in heat transfer, the peak temperature is still approximately 7°C higher compared to the surface cooled cell. In order to further optimise the effectiveness of the tab cooling system, a model is used to reveal the SoC and temperature throughout of the cell with different TMSs, and to further optimize the cell design parameters that enable improved heat transfer while maintaining temperature homogeneity.

***Model validation.***—The 2D thermo-electro model developed was parameterised for each of the three variants of cells following the methodology reported previously.[21] Cell to cell variation in thermal and electrical performance was accounted for by parameterising three variants individually. The geometrical and thermal parameters used in the model are listed in Table I and Table II respectively.

*Adiabatic condition validation.*—The parameterised models were validated against experiments by using the current demand representing the US06 drive cycle under ‘near-adiabatic’ condition, where all exposed surfaces were covered with thermal insulation material. Figure 6 shows the result of the C70 cell. The validation for C30 and S30 cells achieved a similar level of accuracy and is not shown in the manuscript for brevity. Figure 6a shows the current input for the drive cycle, the maximum current is capped at 100 A. Measured versus the simulated terminal voltage are shown in Figure 6b. For the temperature prediction, the model shows good agreement with the experiment, with a maximum absolute error less than 0.6°C. This shows that the overall cell model can accurately represent the heat capacity and heat generation.

*Validation under thermal management.*—To ensure the model can predict the temperature distribution, the cell model of all three cell variants was validated against experiments with the TMS applied. Four experiments were performed in total, where the tab cooling was applied to all the variants and the surface cooling was only applied to the S30 cell.

For surface cooling, the temperature at the top face (width × length) of the cell was maintained at 20°C. For tab cooling, the temperature of both tabs was maintained at 20°C. In both cases, all other exposed surfaces were covered with thermal insulation material to minimise heat loss. The ambient temperature was maintained at 20°C. The cells were allowed to reach thermal equilibrium before the tests. The cells were also charged to 4.2 V until the current dropped below 0.01C (0.16 A) and rested for 2 hours before the test. During the test, the cells were discharged with the constant current rate of 5C (80A) until 2.7 V followed by 2C (32 A) constant current charge until 4.2 V. The three temperature sensors (S1, S2, S3) were placed along the length direction on the centreline. The predicted temperatures at the same locations were compared with these measurements.

Figure 7 shows the simulated temperature at each location versus the experimental measurement. For the S30 surface cooling cell, the maximum error is at S3 location with a difference of + 1.5°C compared to the experiment, as shown in Figure 7a. The maximum error occurs at the temperature peak at the end of discharge. Higher predicted temperature at the S2 and S3 location led to an over-prediction of temperature during the subsequent charging.

For C30 under tab cooling cell, the maximum error observed is approximately −1.5°C and +1.9°C at S1 and S3 respectively. The model predicts a slightly higher usable capacity, indicated by the time at the temperature peak, compared with experiments. This could be caused by the degradation of the experimental cell during the testing, which is not accounted for in the model. For S30 and C70 cells under tab cooling, the model showed very good agreement experiment with a maximum error of less than 1°C against the measured temperatures.

Overall, this validation experiment indicated that the model can predict the temperature distribution of all cells under TMS with an acceptable level of accuracy. The models are next used to reveal cell

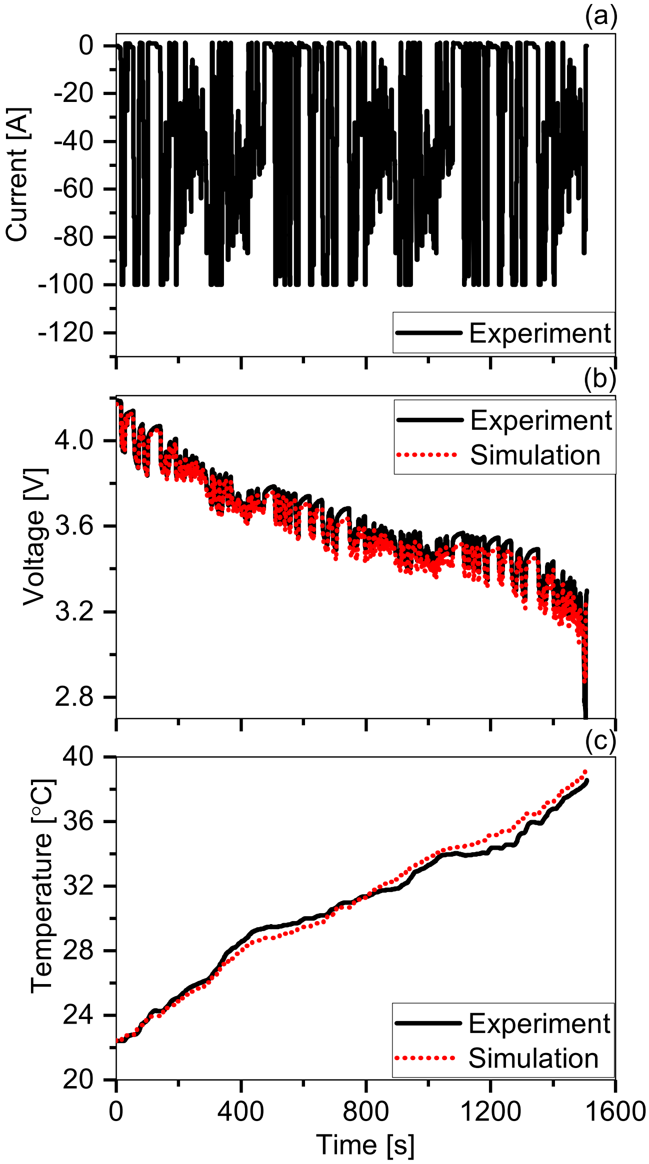


**Figure 6.** Model prediction against experimental measurement under US06 drive cycle for C70 cell: (a) Input current, (b) Cell terminal voltage and (c) Cell temperature at the face centre.

internal states in Internal temperature, current and SoC distribution section.

***Internal temperature, current and soc distribution.***—Figure 8 shows the predicted internal temperature, current and SoC distributions in cells with different types of TMS applied. Snapshots of four internal states are plotted. Times of 'snapshots' taken are different for the tab cooled and surface cooled cells. This is due to the difference in overall discharge time, which is related to the difference in usable capacity caused by the TMS strategy and variation in cell performance. The simulation was performed for the same temperature and current conditions as shown in Figure 7. The result for two cells is presented in Figure 8 in order to compare the performance of the surface cooled cell (S30 -surface cooled) to the best performing tab-cooled cell (C70 – tab cooled).

Figure 8a shows the simulation domain and the exact position of the internal simulation nodes used in each case. For the S30 cell, the surface cooling is applied to the top surface (T = 5.5 mm) and the rest of the surfaces are thermally insulated. The temperature of the surface is controlled at 20°C. For the tab cooled C70, the temperatures at each electrical tab are controlled at 20°C. Figures 8b–8c) plot the difference between the parameter at each point and the mean value of the domain, where mean value of the domain is time varying.

Figure 8b shows the temperature distribution across the thickness and length of the cell, dimensions during the discharge. In all cases, the constant current discharges are terminated when the terminal voltage reaches 2.7V, resulting different discharge duration and usable capacity. The temperatures at which the discharge stopped is used to compare different cooling systems. For the surface cooled cell, the average temperature rises from 20°C to 32°C during the discharge. In comparison, the tab cooled cell temperature rises to 40°C by the end discharge. At t = 440 s for the surface cooled cell and t = 485 s for the tab cooled cell, the average temperature difference is only 4°C. However, this difference increases significantly toward end discharge - approximately 200s later - to 8°C. The tab cooled cell shows higher usable capacity with discharge terminated at t = 730 s, 65 s longer compared to the surface cooled cell.

The S30 surface cooled cell builds up a significant thermal gradient by the end of the discharge with the maximum difference of approximately 11.6°C between the hottest and the coldest part of the cell. The layers close to the cooling surface are around −7.5°C compared to the cell average temperature, while the bottom layer is around +4.1°C compared to the average temperature. By contrast, for the C70 tab cooled cell, the maximum temperature difference is only 2°C. The centre of the cell is + 0.6°C higher than the average and the negative tab end of the cell is −1.4°C lower at the end of the discharge.

The cell impedance is a strong function of temperature. Therefore, a difference in temperature between different parts of a cell can lead to uneven current flow. This uneven current, in turn, lead to a positive feedback loop between temperature and current. For the S30 surface cooled cell, the maximum discharge rate was 2.1C (34A) lower than the average rate of 5C (80A) as shown in Figure 8b. This results in a maximum discharge rate of 7.1C (114 A) for the layers furthest from the surface being cooled. For the C70 tab cooled cell, the maximum discharge rate deviation was only 0.52 C (8 A) lower than the average.

As a consequence of the inhomogeneous current, the SoC at the end of discharge is also uneven. For the surface cooled cell, the 'colder' part of the cell is less discharged, + 6% SoC compared to the average, while the hotter part of cell is disadvantaged by 1.1% more compared to the average SoC. In case of the tab cooling cell, SoC varies by a maximum 0.6% across the cell.

***Parameter study on existing cells.***—The experimental results of C70 shows significant improvement compared to the C30 and S30 variants under tab cooling. This confirms that a larger cross-sectional area at electrical tabs improves the effectiveness of the tab cooling strategy. The internal states prediction shows that the tab cooling strategy provides much more uniform temperature distribution, which results in a more homogenous current and SoC distribution. However, tab cooling is still limited by its overall heat removal capability due to surface area for conduction.

In this section, the geometrical parameters which could potentially improve the heat transfer through the tabs are investigated. The effect of tab width, tab thickness and the thickness of current collectors are analyzed using the model. Figure 9a shows the parameters that are explored. To quantify the impact of a design, the average, maximum and minimum temperature of the cell at the end of a 5C (80 A) discharge are used as the key performance indicators.

Altering the geometrical parameters can lead to change in the cell mass and potentially cell electrochemical performance. To understand the implication of changing a parameter, the energy density of the cell is recalculated according to the change. Since the investigated geometrical changes are not related to the electrode material and geometry of the cell electrode stack, it is assumed that the energy density is only affected through a modified in cell mass whereas the energy content in watt-hour is not affected by this change.

For this section, the cell model for the C70 variant is used as a baseline. The geometrical parameters for C70 are modified accordingly while the electrical and thermal parameters are unchanged. The

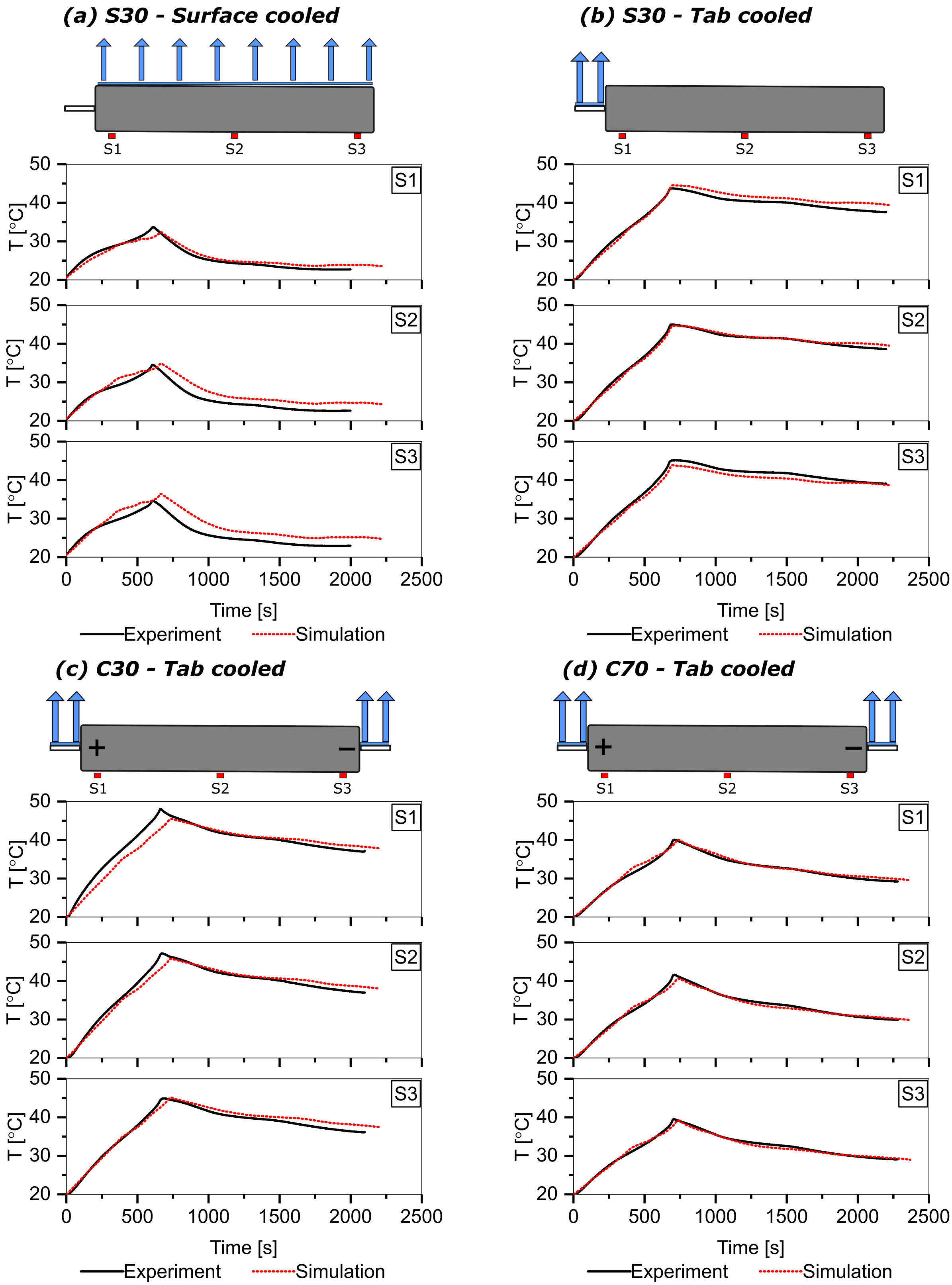


**Figure 7.** Temperature measurement along the length of cell (S1-S3) during constant current 5C discharge and 2C charge: (a) surface cooled S30 cell; (b) tab cooled S30 cell; (c) tab cooled C30 cell and (d) tab cooled C70 cell.

geometrical property of the baseline cell (C70) is shown in Table IV. The baseline cell energy density is 210 Wh/kg, which is obtained by measuring cell mass and energy content under 0.1C (1.6 A) full depth discharge.

For tab thickness and CC thickness, the value of the parameter is increased by up to 90% from the baseline value. The possible tab width range is constrained by the physical size. Each parameter is varied independently to the other two, Figures 9b–9d.

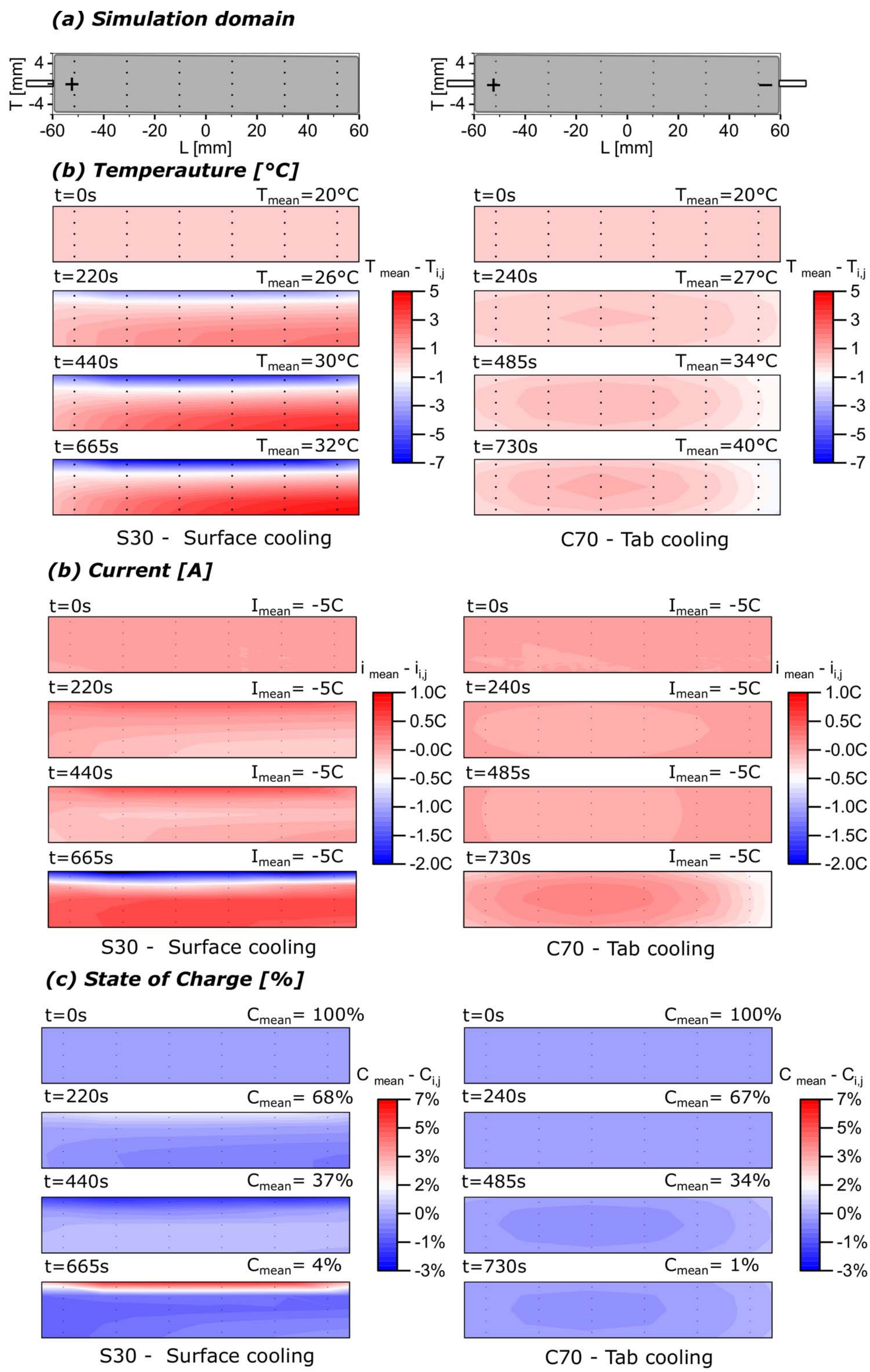


**Figure 8.** Cell internal states over a 5C constant current discharge: (a) Simulation domain, (b)Temperature distribution, where black dots are simulation nodes, (c) Current distribution and (d) SoC distribution.

Figure 9b shows the effect of tab width on the cell average, maximum and minimum temperature during the discharge. To provide a reference for the analysis, the average temperature of the S30, C30 and C70 cell measured experimentally under tab cooling system are also plotted. These references are used as a validation between the model prediction and the experimental measurement when a geometrical parameter is changed. As the C70 cell model is used, it is expected that the prediction of cell temperatures are closely matched with experimental measurement when the tab width is 70 mm. For the S30 cell, the measured temperature is 0.5°C higher than the simulation. For the C30 cell, the predicted value is 2°C lower than the experimental value. Overall, the experimental average temperatures show good quantitative match with model prediction.

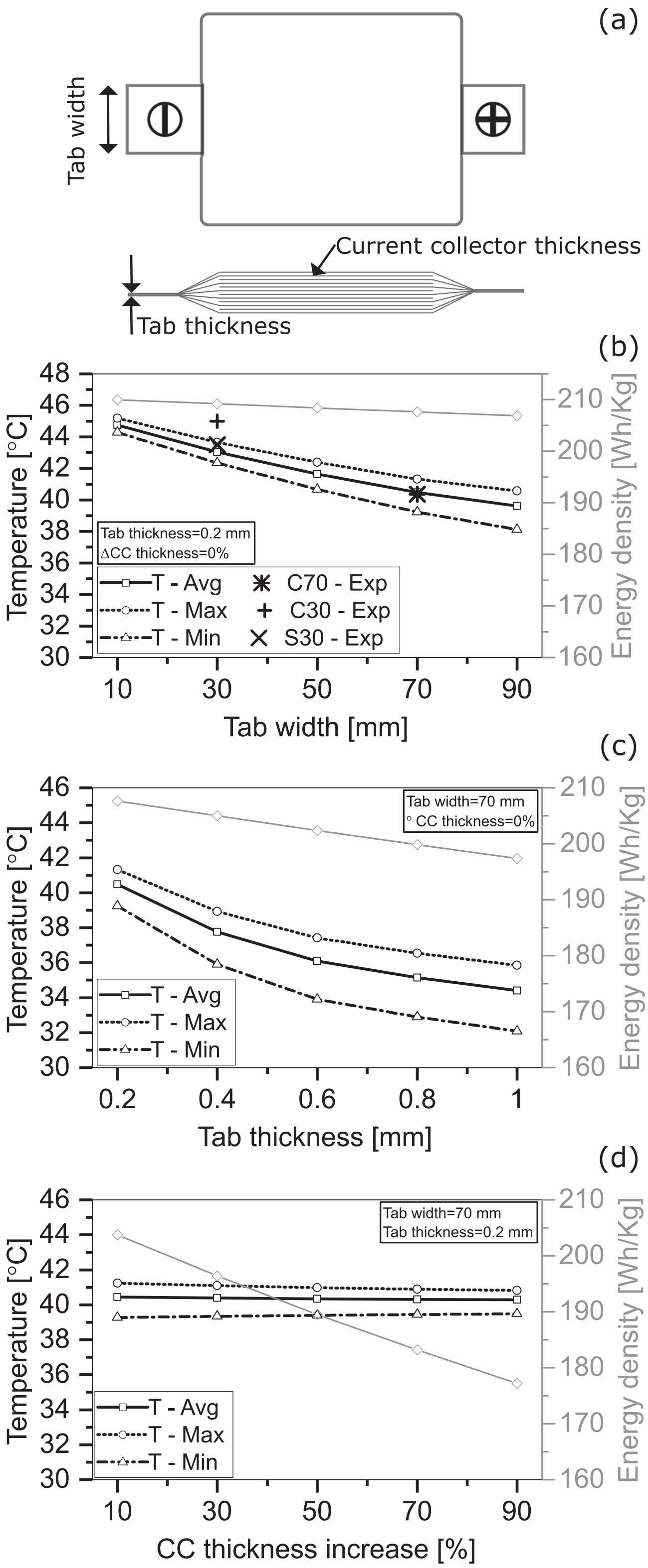


**Figure 9.** Influence of geometrical parameters on tab cooling system performence: (a) Parameters studied, (b) Tab width, (c) Tab thickness and (d) Current collector(CC) thickness.

With tab width increased from 10 mm to 90 mm, the average temperature at the end of discharge is reduced from 44.5°C to 39.5°C, as shown in Figure 9b. The mass increase due to wider tabs choice has reduced the energy density from 210 Wh/kg to 207 Wh/kg. At the same time, the maximum temperature difference along the length of the cell is increased from 1°C to 2.4°C.

**Table IV. The baseline and the range for each parameter.**

| Parameter | Baseline | Analysis range |
|---|---|---|
| Tab width | 70 mm | 10–90 mm |
| Tab thickness | 0.2 mm | 0.2–1 mm |
| Current collector thickness - anode | 10 μm | 10%–90% increase |
| Current collector thickness - cathode | 20 μm | 10%–90% increase |

With tab thickness increases from 0.2 mm (baseline) to 1 mm, the average temperature is reduced from 40.4°C to 34.4°C. Improvement in the heat transfer pathway at the tab has led to an increase in the rate of heat transfer along the current collector. This lead to an increase of thermal gradient along the length of the cell, with the maximum temperature difference increased from 2°C to 3.7°C. Similar to the width change, the thickness increase lead to reduction of cell level energy density from 210 Wh/kg to 197 Wh/kg, as shown in Figure 9c.

Figure 9d shows the effect of current collector thickness on the thermal performance. In this analysis, the thickness of current collectors is increased, proportionally to the baseline values, 10 μm (anode) and 20 μm (cathode). The thickness increase has little effect on the average temperature of the cell, which dropped by only 0.25°C for a 90% increase from the baseline. The temperature difference along the cell length reduced from 2°C to 1.5°C for 10% to 90% increase. This is expected as thicker current collectors improve the in-plane heat transfer. However, the current collector thickness increase has a significant impact on energy density due to its mass increase. The energy density drops to 177 Wh/kg with a 90% increase from 203 Wh/kg with a 10% increase. The result shows that the current collector thickness in the current configuration of 70 mm tab width and 0.2 mm tab thickness is not the thermal 'bottleneck'.

The parameter study indicates the thermal 'bottleneck' is still the cross-sectional area of the tabs for this cell. By increasing the cross-sectional area, the thermal performance of tab cooling system can be brought to a comparable level with surface cooled system while maintaining the benefit of the minimal thermal gradient. As an example, for tab thickness = 1 mm, the thermal performance is comparable with the surface cooled cell, where the average temperature at the end of discharge is 32°C. With the same average temperature compared to surface cooling, the tab cooling system induced a much smaller thermal gradient of 3.7°C across the cell compared to 11.6°C in the surface cooling case.

This thermal 'bottleneck' exists predominantly due to a mismatch between the total current collector and tab cross-sectional area. A simple calculation shows the scale of the mismatch. The total cross-sectional area of the current collectors for one electrode is given by:

$$CSA_{cc} = N_{cc} \times T_{cc} \times W_{tab} \quad [3]$$

Where $CSA_{cc}$ is the total cross-sectional area of all current collectors for one electrode, $N_{cc}$ is a number of current collector layers, $T_{cc}$ is the thickness of a current collector and $W_{tab}$ is the width of the electrical tab.

The tab cross-sectional area is given by:

$$CSA_{tab} = T_{tab} \times W_{tab} \quad [4]$$

Where $CSA_{tab}$ is the total cross-sectional area of one tab, $T_{tab}$ is the thickness of the electrical tab and $W_{tab}$ is the width of the electrical tab.

It is assumed that the width of the electrode sheet at the welding point is the same as the width of the tab. The calculation result is shown in Table V. The mismatch between the total current collector cross-sectional area is apparent, with the $CSA_{tab}$ being over three times smaller than the $CSA_{cc,pos}$. Therefore, to eliminate the 'bottleneck', the cross-sectional area at the tabs need to match the total cross-sectional area of each current collector as a minimum.

**Table V. Cross-sectional area for current collectors and tab.**

| | Cross-sectional area [$mm^2$] |
|---|---|
| $CSA_{cc,neg}$ | 26.6 |
| $CSA_{cc,pos}$ | 51.8 |
| $CSA_{tab}$ | 14.0 |

***Design and optimisation by extrapolating the model for a different form factor.***—So far, we show that tab cooling can have comparable thermal performance with surface cooling while keeping the thermal gradient at a minimum by simply optimising the cell tab design. However, these conclusions were made on a cell with an aspect ratio (Length/Width) close to one. However, pouch-type cells with higher aspect ratio are becoming more popular for automotive battery packs due to packaging constraint in floor height of the vehicle. The pouch cells tend to be in a long rectangular shape with tabs on the opposing side. Compared to a cell with a higher aspect ratio, the cells studied in this work have a shorter distance for the thermal gradient to develop in the length direction. To further explore the suitability of using tab cooling in a high aspect ratio, a virtual cell and its energy density is created using the model. The geometrical dimension of the virtual cell is similar to that of the E63 cell manufactured by LG Chem.

The geometrical dimension of the virtual automotive cell is shown in Figure 10a, with an aspect ratio of approximately 2.6. The thickness of the cell is the same as the custom cell (S30, C30 and C70). The electrochemical model parameters are scaled based on the C70 cell, according to Equation 1 and Equation 2. The virtual cell capacity is 51.3 Ah. Based on the parameter study, the tab design of the virtual cell is optimised to improve the tab cooling performance. The electrical terminal of the virtual cell is 1.5 mm in thickness and 100 mm in width.

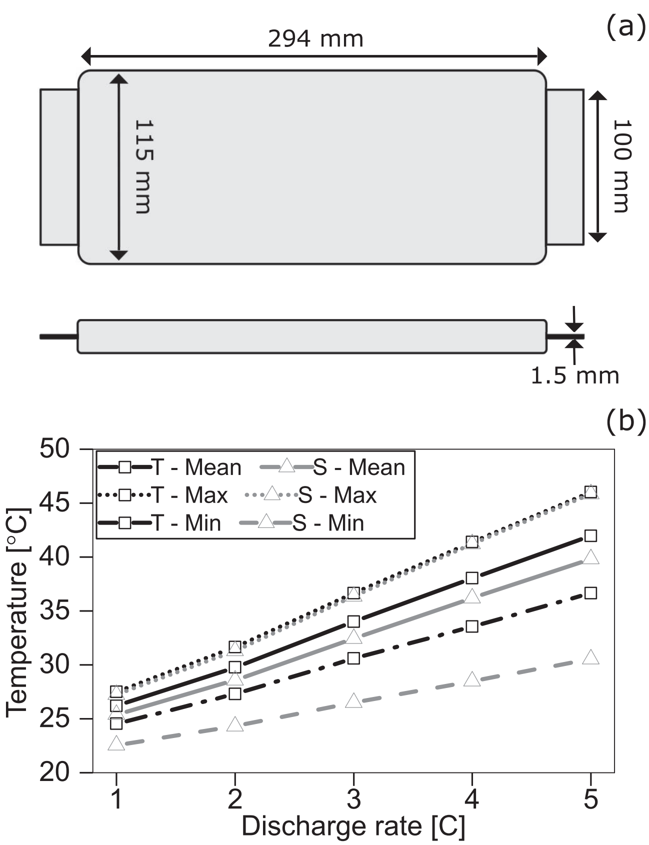


**Figure 10.** Predicted tab and surface cooling comparison for an automotive cell design: (a) Cell format and (b) Temperature distribution over different discharge rates, where T – tab cooled and S – surface cooled.

The thicker tabs result in a 3.9% reduction in the cell level energy density compared with standard tab thickness of 0.2 mm. A further improvement was made to tab welding thermal resistance, assuming the thicker tab will lead to better thermal contact (how this would be achieved during manufacturing has not been studied and is not known).[39]

The end-of-discharge temperature distribution under tab cooling and surface cooling strategies are presented. The performance of the two TMS strategies is compared across a range of discharge rates, 1C (48 A) to 5C (240 A) at 1C (48 A) increments. Figure 10 shows the maximum, minimum and average temperature of the cell at the end of discharge for each cooling method.

The tab cooled cell has similar average temperature as the surface cooled cell, with the tab cooled cell only 0.8°C hotter at 1C and 2.1°C at 5C. Both cells have similar peak temperature across the range of discharge rates. However, the tab cooled cell causes a significantly less thermal gradient. The maximum temperature gradient at 1C is 3°C for tab cooled cell and 5°C for surface cooled cell, 66% higher. At 5C, tab cooling induces a 10°C thermal gradient. In comparison, the surface cooled cell has 17°C difference across the cell, a 70% increase.

This shows that with a simple modification to the tab geometry, a tab cooling system can achieve a heat rejection performance similar to surface cooling while maintaining the advantage of reducing thermal inhomogeneity. A combination of better heat rejection and better temperature uniformity should lead to improved cell life, in comparison to the surface cooled system. The proposed change to the cell tab design has a minor impact on the cell gravimetric energy density. However, there is a significant opportunity for these cell-level energy densities to be recouped at the battery pack level. Firstly, through increases in useable capacity caused by reduced inhomogeneities within the cell. Secondly, TMSs based on tab cooling can be more compact than cooling plates between every other cell are not required. Thirdly, the potential longer life of the battery pack means the system will need less redundant capacity at the start of life, therefore lead to reduced cost and weight at pack level.

## Conclusions

This work used customised lithium-ion cells designed with varying electrical tab width and position to investigate the ways to optimise a tab cooling thermal management strategy. The cells were characterised to quantify the improvement in the thermal transfer pathway due to wider tab widths.

Using custom made cells, it was shown that increasing the cross-sectional area of the tab can lead to significant improvement in heat transfer between cell-stack and the tabs. The experiments indicate that increasing the tab width from 30 mm to 70 mm can lead to a 14% reduction in cell peak temperature under aggressive discharge. However, it showed that tab cooling was still much less capable of removing heat than surface cooling for these cells.

A 2D electro-thermal model was parameterised and validated for the custom cells used in this study. The model was used to explore internal distributions of temperature, current and SoC. It showed that the best performing cell for a tab cooling strategy is still less capable of removing heat compared with the surface cooled cell. However, tab cooling still provides significant benefit in maintaining thermal, current and SoC uniformity. The surface cooled system induces a thermal gradient across cell thickness over 5 times greater compared with the tab cooling system.

The model shows that the existing thermal ‘bottleneck’ between cell electrode stack and the electrical tabs can be substantially reduced by increasing the cross-sectional area of the electrical tabs. A virtual cell with a high aspect ratio and high capacity (based upon the LG Chem E63 cell) was modelled to explore the feasibility of using tab cooling strategy in large format cells and demonstrates the same result should be possible for cells of this shape and size.

For the first time, we show that tab cooling can be as effective as conventional surface cooling while maintaining the benefits of increased thermal uniformity. However, existing cells need to be re-designed to achieve this. We found that the optimisation of the cell design only needs to be done at the electrical tabs, by only re-designing the width, thickness, position and weld of the tabs to the current collectors. There is no need to alter the design of cell electrode stacks in any other way. This would potentially allow wider adoption of tab cooling and enable longer battery life.

## Acknowledgment

We acknowledge the funding support received from the BIAM-Imperial Centre for Materials Characterisation, Processing and Modelling at Imperial College London. The work was also supported by the EPSRC TRENDS project (grant number EP/R020973/1) and the Innovate UK BATMAN project (grant number 104180). This work was partially carried out with funding from the Faraday Institution (grant number EP/S003053/1, FIRG003). We acknowledge Thermal Hazard Technology for their assistance for measuring cell heat capacity. We also thank Dr Monica Marinescu for her generous comments on manuscript.

## ORCID

Yan Zhao https://orcid.org/0000-0002-3211-6740
Laura Bravo Diaz https://orcid.org/0000-0002-0259-8590
Yatish Patel https://orcid.org/0000-0001-7828-5315
Teng Zhang https://orcid.org/0000-0002-3657-5151
Gregory J. Offer https://orcid.org/0000-0003-1324-8366

## References

1. I. E. A. International and E. Agency (2018).
2. Y. Dai, L. Cai, and R. E. White, *J. Electrochem. Soc.*, **161**, E3348 (2014).
3. X. Feng, J. Sun, M. Ouyang, X. He, L. Lu, X. Han, M. Fang, and H. Peng, *J. Power Sources*, **272**, 457 (2014).
4. B. Wu, V. Yufit, M. Marinescu, G. J. Offer, R. F. Martinez-Botas, and N. P. Brandon, *J. Power Sources*, **243**, 544 (2013).
5. Y. Zhao, Y. Patel, I. A. Hunt, K. M. Kareh, A. A. Holland, C. Korte, J. P. Dear, Y. Yue, and G. J. Offer, *J. Energy Storage*, **13**, 296 (2017).
6. J. Remmlinger, S. Tippmann, M. Buchholz, and K. Dietmayer, *J. Power Sources*, **254**, 268 (2014).
7. P. Ramadass, B. Haran, R. White, and B. N. Popov, *J. Power Sources*, **112**, 614 (2002).
8. T. G. Zavalis, M. Klett, M. H. Kjell, M. Behm, R. W. Lindström, and G. Lindbergh, *Electrochim. Acta*, **110**, 335 (2013).
9. R. Zhao, S. Zhang, J. Gu, J. Liu, S. Carkner, and E. Lanoue, *J. Power Sources*, **255**, 29 (2014).
10. Z. Ling et al., *Renew. Sustain. Energy Rev.*, **31**, 427 (2014).
11. R. W. Van Gils, D. Danilov, P. H. L. Notten, M. F. M. Speetjens, and H. Nijmeijer, *Energy Convers. Manag.*, **79**, 9 (2014).
12. M. Klein, S. Tong, and J. W. Park, *Appl. Energy*, **165**, 639 (2016).
13. T. M. Bandhauer, S. Garimella, and T. F. Fuller, *J. Electrochem. Soc.*, **158**, R1 (2011).
14. E. Mcturk, T. Amietszajew, J. Fleming, and R. Bhagat, *J. Power Sources*, **379**, 309 (2018).
15. B. Wu, Z. Li, and J. Zhang, *J. Electrochem. Soc.*, **162**, A181 (2014).
16. K. F. Yeow and H. Teng, *SAE Int. J. Alt. Power.*, **2**, 179 (2013).
17. Y. Troxler, B. Wu, M. Marinescu, V. Yufit, Y. Patel, A. J. Marquis, N. P. Brandon, and G. J. Offer, *J. Power Sources*, **247**, 1018 (2014).
18. I. Hunt, T. Zhang, Y. Patel, M. Marinescu, A. Swiatek, and G. J. Offer, *J. Electrochem. Soc.*, **165**, 6073 (2018).
19. I. A. Hunt, Y. Zhao, Y. Patel, and G. J. Offer, *J. Electrochem. Soc.*, **163**, A1846 (2016).
20. M. Klein, S. Tong, and J. W. Park, *SAE Tech. Pap.*, **1** (2014).
21. Y. Zhao, Y. Patel, T. Zhang, and G. J. Offer, *J. Electrochem. Soc.*, **165**, A3169 (2018).
22. A. Samba, N. Omar, H. Gualous, O. Capron, P. Van Den Bossche, and J. Van Mierlo, *Electrochim. Acta*, **147**, 319 (2014).
23. J. Li, Y. Cheng, L. Ai, M. Jia, S. Du, B. Yin, S. Woo, and H. Zhang, *J. Power Sources*, **293**, 993 (2015).
24. W. Zhao, G. Luo, and C. Y. Wang, *J. Power Sources*, **257**, 70 (2014).
25. U. S. Kim, C. B. Shin, and C. S. Kim, *J. Power Sources*, **180**, 909 (2008).
26. B. Rieger, S. V. Erhard, S. Kosch, M. Venator, A. Rheinfeld, and A. Jossen, *J. Electrochem. Soc.*, **163**, A3099 (2016).
27. D. A. H. McCleary, J. P. Meyers, and B. Kim, *J. Electrochem. Soc.*, **160**, A1931 (2013).
28. U. S. Kim, C. B. Shin, and C. S. Kim, *J. Power Sources*, **189**, 841 (2009).
29. G.-H. Kim, K. Smith, K.-J. Lee, S. Santhanagopalan, and A. Pesaran, *J. Electrochem. Soc.*, **158**, A955 (2011).
30. M. Guo, G. H. Kim, and R. E. White, *J. Power Sources*, **240**, 80 (2013).
31. R. Spotnitz and J. Franklin, *J. Power Sources*, **113**, 81 (2003).
32. John Newman and W. Tiedemann, *J. Electrochem. Soc.*, **140**, 1961 (1993).
33. H. Gu, *J. Electrochem. Soc.*, **130**, 1459 (1983).
34. K. H. Kwon, C. B. Shin, T. H. Kang, and C. S. Kim, *J. Power Sources*, **163**, 151 (2006).
35. Y. Troxler, B. Wu, M. Marinescu, V. Yufit, Y. Patel, A. J. Marquis, N. P. Brandon, and G. J. Offer, *J. Power Sources*, **247**, 1018 (2014).
36. R. Jackey, M. Saginaw, P. Sanghvi, J. Gazzarri, T. Huria, and M. Ceraolo, *MathWorks*, 1 (2013).
37. T. Huria, M. Ceraolo, J. Gazzarri, and R. Jackey, 2012 *IEEE Int. Electr. Veh. Conf.*, 1–8 (2012).
38. P. Taheri and M. Bahrami, *SAE Int. J. Passeng. Cars - Electron. Electr. Syst.*, **5**, 2012-01–0334 (2012).
39. A. Hales, L. B. Diaz, M. W. Marzook, Y. Zhao, Y. Patel, and G. Offer, *J. Electrochem. Soc.*, **166**, A2383 (2019).